

We are IntechOpen, the world's leading publisher of Open Access books Built by scientists, for scientists

6,900

Open access books available

186,000

International authors and editors

200M

Downloads

Our authors are among the

154

Countries delivered to

TOP 1%

most cited scientists

12.2%

Contributors from top 500 universities



WEB OF SCIENCE™

Selection of our books indexed in the Book Citation Index
in Web of Science™ Core Collection (BKCI)

Interested in publishing with us?
Contact book.department@intechopen.com

Numbers displayed above are based on latest data collected.
For more information visit www.intechopen.com



Quantum Transport and Quantum Information Processing in Single Molecular Junctions

Tomofumi Tada
*Department of Materials Engineering, Global COE for Mechanical System Innovation,
The University of Tokyo
Japan*

1. Introduction

Superposition states and entanglement in quantum bits (qubits) are inherently required in quantum computations (Benenti et al., 2004; Miyano & Furusawa, 2008; Nielsen & Chuang, 2004; Sagawa & Yoshida, 2003). Electron and nuclear spins have been identified as attractive candidates for qubits (Ladd et al., 2010), and the prominent properties involved in quantum spins have been observed in liquid state molecules (Vandersypen et al., 2001) and solid state materials such as doped silicon (Kane, 1998) and nitrogen-vacancy (NV) center in diamond (Childress et al., 2006). An impressive demonstration of quantum computations on Shor's algorithm was carried out by Vandersypen and co-workers by using a liquid state system, in which each molecule includes seven nuclear spin qubits (Vandersypen et al., 2001). The operations for single and double qubits were implemented through bulk nuclear magnetic resonance (NMR) technique, in which radio-frequency (RF) pulse sequences were constructed so as to manipulate nuclear spin states along the design of quantum gates for the factorization. The RF pulse applications were succeeded in the precise control of nuclear spin states, and in turn in the factorization of a small number ($N=15$) in Shor's algorithm. However, the liquid NMR signals are inherently averaged signals from a huge number of molecules, and therefore problems on initialization of qubits and pseudo-entanglement appear in the liquid NMR system, which make the liquid system difficult for the quantum computations using a larger number of qubits, although the operations in NMR are in principle robust.

The difficulties lying on the spin ensemble study are resolved when operations and readout are implemented on a single spin. Optical excitation and fluorescence of a single electron spin of NV center in diamond are powerful for the observations of coherent dynamics and readout of the single electron spin states (Cappellaro et al., 2009; Childress et al., 2006; Jacques et al., 2009; Jelezko et al., 2004a;b; Neumann et al., 2008; Smeltzer et al., 2009). The microwave (MW) and RF pulses designed by taking the hyperfine structures into account also lead to the robust control and readout of single/few nuclear spin states. Besides, the multiparticle entanglement among single electron/nuclear spins was confirmed in the NV center (Neumann et al., 2008).

The electron-nuclear spins for qubits have been investigated extensively also in P-doped silicon, which has a field effect transistor (FET) structure (Kane, 1998; Lo et al., 2007; McCamey et al., 2006; Mccamey et al., 2009; Morton et al., 2008; Stegner et al., 2006). In Kane's silicon-based quantum computer, the two kinds of gates, named as A- and J-gates, were

introduced to control the resonance frequency of a ^{31}P nuclear spin and electron-mediated couplings between adjacent nuclear spins, respectively (Kane, 1998). In the silicon systems, the electrical detection of ^{31}P nuclear spin states is also possible. The hyperfine interactions between electron and ^{31}P nuclear spins are again key interactions for the control and readout of spin states. These pioneering works show that the electron-nuclear spin pairs in solid state materials have prerequisite properties for quantum computations, and that we can observe and control the quantum properties in practical ways.

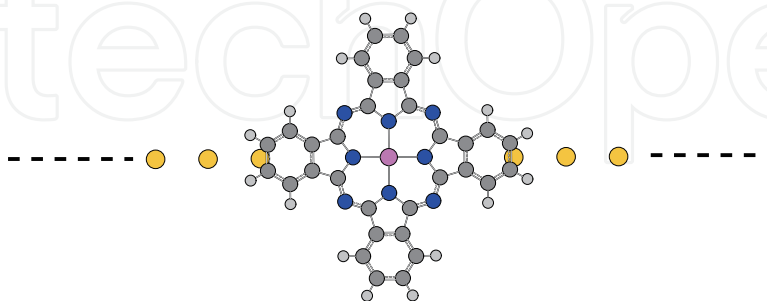


Fig. 1. Single molecular junction composed of a Cu-phthalocyanine molecule and one-dimensional gold chain. The yellow, dark gray, light gray, blue, and purple atoms are gold, carbon, hydrogen, nitrogen, and copper, respectively.

Another key issue for the design of quantum computers is high scalability. The NV center in diamond and doped-silicon systems of course have scalable designs in its original concept because the operation and readout of single/few spin(s) in these systems are available and highly robust. However, we have to *perfectly* control the doping of P in Si and NV center in diamond in terms of the concentration and doping positions to realize the solid state quantum computers including many qubits. This is not a trivial task if we use a top-down fashion from bulk materials. On the other hand, bottom-up approaches have been succeeded in the fabrication of the one-dimensional atomic chains and molecular chains between electrodes or on substrates (Carroll & Gorman, 2002; Joachim, 2000). For example, a well-defined one-dimensional structure composed of gold atomic chains and a metal-phthalocyanine molecule (Fig. 1) on NiAl(110) surface (Nazin et al., 2003) has a large feasibility for high-scalable and well-defined spin arrays by repeating the same junction structure on a substrate through self-assembling processes. Since a single organic molecule can be the source of electron and nuclear spins and one-dimensional atomic chains connected to the single molecules will be useful for electrical detection of spin states, the spin array structure composed of single molecular junctions (see Fig. 2) is a new candidate for the device structure designed for quantum computations with high scalability. Here we use the term *single molecular junctions* to express the nano-scale junctions composed of a single molecule and electrodes. However, despite the potential ability in this type of device structures, the investigations of molecular junctions intended for quantum computations seldom have been reported so far (Tada, 2008). Therefore this chapter is devoted to investigate the possibility of operation and readout of single spins in molecular junctions in the framework of the first principles electronic structure calculations.

This chapter is organized as follows; Section 2: the introduction for the classical and quantum computers, Section 3: the control of spin states using the rotating magnetic field, Section 4: the electronic conduction in single molecular junctions, and Section 5: the operation-readout

robust switching of a single nuclear spin in the single molecular junctions for the quantum information processing.

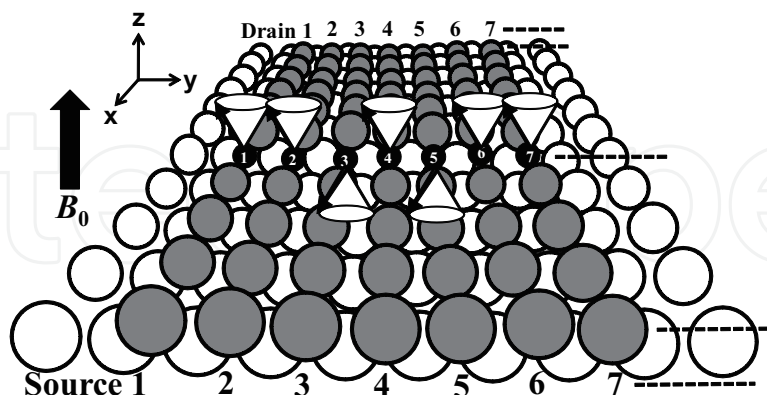


Fig. 2. Schematic of the solid-state nuclear-spin (black) array on a substrate (white). The gray symbols are atoms in electrodes connected to the nuclear spins.

2. Classical computers and quantum computers

2.1 Classical and quantum bits

To briefly understand the difference between the classical and quantum computers, let us consider three classical/quantum bits in an electronic device. The information of “0” or “1” can be stored in a classical bit, whereas a superposition state (e.g., “0+1”) can be allowed in a quantum bit (qubit). In the three classical bits, the eight combinations (i.e., “0,0,0”, “0,0,1”, “0,1,0”, “0,1,1”, “1,0,0”, “1,0,1”, “1,1,0”, “1,1,1”) can be realized, but the bit information we can store concurrently is just a single combination (e.g., “0,0,1”). When an operation A is operated to the eight combinations, the eight operations of A in a sequential manner are required in the classical three bits device. On the other hand, in the three qubits device, we can prepare the eight combinations concurrently by using the superposition states (i.e., “0+1,0+1,0+1” \rightarrow the eight combinations). Thus the eight operations of A in the classical bits can be reduced to a single operation A in the three qubits device. When the number of bits increases much more, the advantage of quantum computers is absolutely obvious. We thus sometimes call the quantum computer the *super-parallel* computer.

2.2 Classical and quantum logic gates

The electronic circuits in electronic devices currently used are designed on the basis of the classical logic gates. The “AND” and “NOT” gates shown in Fig. 3(a) are the typical classical gates, in which the input of two/one bit information is converted to a single bit as an output in the “AND”/“NOT” gate. It is well-known that any logic gates in classical computers can be constructed from the “AND” and “NOT” gates. In quantum computers, on the other hand, the “unitary (U)” and “controlled-NOT (c-NOT)” gates are the key logic gates in the quantum computations (Benenti et al., 2004; Miyano & Furusawa, 2008; Nielsen & Chuang, 2004; Sagawa & Yoshida, 2003). Fig. 3(b) shows the rules in the bit transformation of the U and c-NOT gates. The characteristic properties in these quantum gates are (i) a superposition state is generated in the U gate, and (ii) the entanglement of the arbitrary two qubits are necessary

for the c-NOT gate. Thus the next concern is how we should realize the two quantum gates in physical systems.

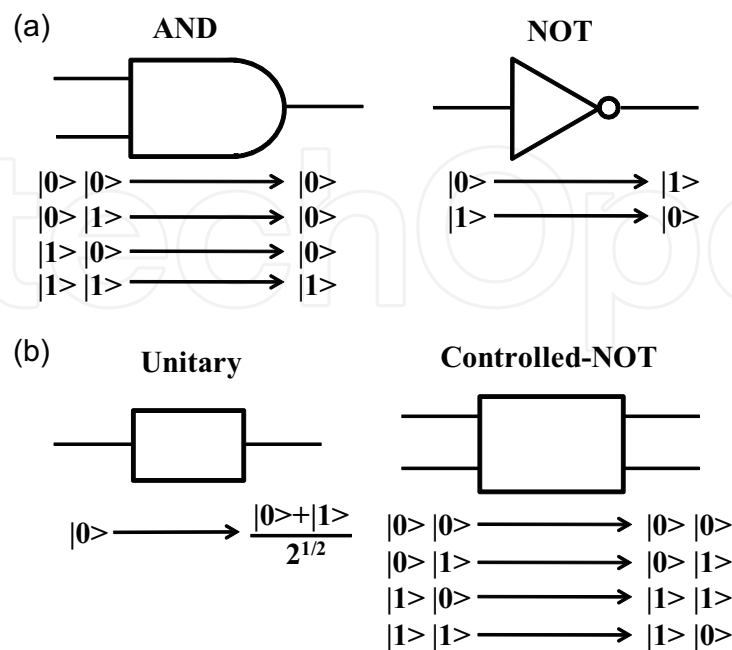


Fig. 3. Schematic of the typical logic gates and the rules of the bit transformation in (a) classical computers and in (b) quantum computers

The trapped ion/atom, nuclear/electron spins, and superconducting charge/phase bit have been extensively investigated as the potential candidates for the qubit, and the superposition and entanglement properties have been confirmed in these systems. In addition to the two properties (superposition and entanglement), the ability for the retention of the qubit information is also an important property for robust systems. According to the review by Ladd and co-workers (Ladd et al., 2010), the nuclear spin of ^{29}Si in ^{28}Si shows the longest T_2 time among the trapped ion/atom, nuclear/electron spins, and superconducting charge/phase bit; T_2 is the phase coherence time and hence T_2 is the measure of the ability of the retention time. The long coherence (25 s of T_2 in ^{29}Si nuclear spin) is the result of the weak interactions between the nuclear spin and its environment. Therefore, the nuclear spins are quite attractive target for the qubit in terms of the long retention time.

3. Control of the nuclear spin states using a rotating magnetic field

3.1 Unitary and controlled NOT gates

Since the advantage of nuclear spins for the retention of qubit information is described in the previous section, let us next consider how we can operate the nuclear spin states. Figure 4 shows a single nuclear spin of $1/2$ in the static magnetic field of B_0 directed to the z-axis. In the condition, the nuclear spin states split into the two states, $s_z = +1/2$ and $-1/2$, and the states can be recognized as "0" and "1" for the bit information. To use the nuclear spin as a qubit, a superposition state of "0" and "1" is required through the unitary transformation (U-gate). The application of a rotating magnetic field B_1 perpendicular to B_0 enables us to operate the nuclear spin. In the presence of the rotating magnetic field B_1 with the angular

velocity of ω , the Hamiltonian is written as

$$H = -\gamma[B_0s_z + B_1\{(\cos\omega t)s_x + (\sin\omega t)s_y\}], \quad (1)$$

where γ is an effective g -factor for the nucleus. Using the time-dependent Schrödinger equation $i\hbar[d|\psi(t)\rangle/dt] = H|\psi(t)\rangle$ and a rotating reference frame $|\psi(t)\rangle = \exp(i\omega ts_z)|\phi(t)\rangle$, the wave function of the nuclear spin can be written as

$$|\phi(t)\rangle = \exp\{it/\hbar[(\gamma B_0 - \hbar\omega)s_z + \gamma B_1s_x]\}|\phi(0)\rangle. \quad (2)$$

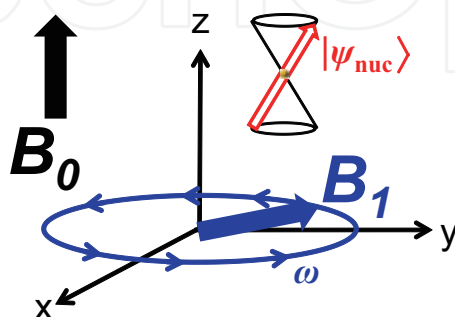


Fig. 4. Single nuclear spin of 1/2 in the static magnetic field B_0 and rotating magnetic field B_1 with the angular velocity of ω .

This equation reveals that when we apply a magnetic field B_1 with $\omega = \gamma B_0/\hbar$, the time dependence of the wave function is completely controlled by the magnetic field B_1 , and thus any superposition state of “0” and “1” can be generated by tuning the application period of the rotating magnetic field (Sagawa & Yoshida, 2003). Since the γ depends on the kinds of the nuclei and its environment, the unitary transformation can be carried out in a selective manner.

The c-NOT operation is feasible by using the spin-spin interaction J between two nuclear spins, leading to the interaction term $Js_z^1s_z^2$ in the Hamiltonian, where s_z^1 and s_z^2 are the spin components along the z-axis for the first and second nuclear spins, respectively. Since Js_z^1 can be regarded as an effective magnetic field for the second nuclear spin, a rotating magnetic field being in resonance to the spin-spin interaction is useful to rotate the second nuclear spin with respect to the first nuclear spin. The magnitude of the spin-spin interaction J depends on the selected two spins, and thus the selective c-NOT is in principle possible.

3.2 Liquid state NMR for quantum computations

Vandersypen and co-workers reported that the nuclear magnetic resonance (NMR) technique is useful for the unitary transformation and c-NOT operations, and that the factorization of a small number ($N=15$) in Shor’s algorithm was succeeded in the application of the radio-frequency (RF) pulse sequence designed for factorization (Vandersypen et al., 2001). Figure 5 shows the seven qubits molecule used in the NMR quantum computations. According to Vandersypen’s study, the resonance frequencies ($\omega/2\pi$) for F(2), F(3), C(6), and C(7) are 0.4895, 25.0883, -4.5191 , and 4.2443 kHz, respectively, and those for J-couplings between F(2)-F(3), F(2)-C(7), F(1)-C(7) are 0.0039, 0.0186, and -0.2210 kHz, respectively. The selective operations on each qubit and on the coupled two qubits are supported in the

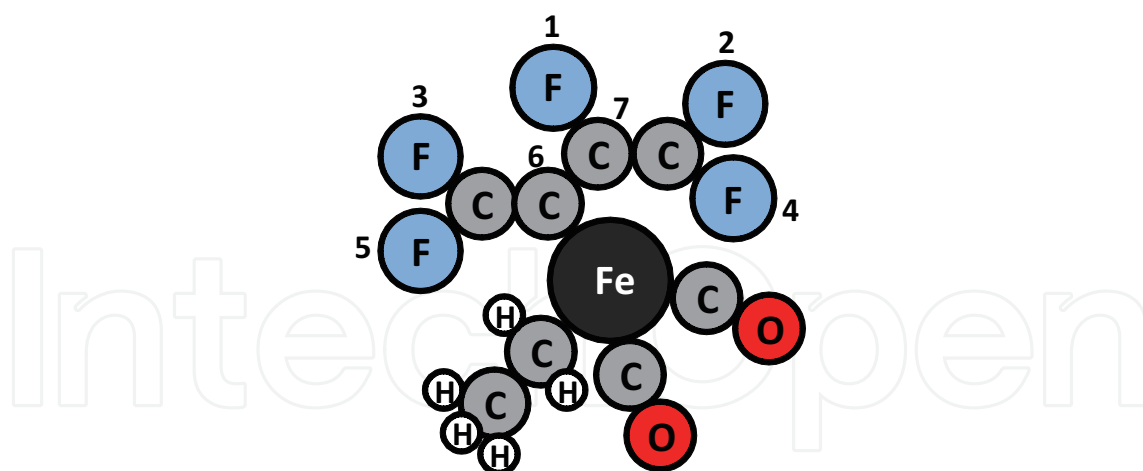


Fig. 5. Seven-bits organic molecule used in the liquid-NMR quantum computations. The numbered atoms are the qubits used in the quantum computations.

magnetic resonance conditions. If we can use a larger molecule designed for a large number of qubits, we may think that such a large molecule is a promising candidate for a practical quantum computer. However, the large molecule including a large number of qubits has a problem that the resonance frequencies for qubits become closer with each other, resulting in the difficulty in the selective operations. In addition, we have to pay attention to the situation that the NMR experiments are carried out in the liquid phase, and therefore the NMR system includes the huge number of the qubit molecules. At the initial stage of the quantum computations, we have to prepare a suitable initialized state for the qubits. When the number of qubits in a molecule becomes larger, the procedure for the initialization becomes more complicated and time consuming. Thus, it is now believed that a molecule including 10-qubits is the largest molecule available for the liquid NMR quantum computations.

3.3 Solid state NMR for quantum computations

The difficulties involved in the liquid NMR systems will be resolved when operations and readout are implemented on a single nuclear spin. The ^{13}C -NMR studies of the NV center in diamond show the powerfulness of the solid state NMR for the applications in quantum computations. However, as described in Introduction, to construct the practical solid state quantum computers, we have to perfectly control the positions of the nuclear spins in diamond. The probability of the precise control in the atomistic level is quite doubtful if we use a top-down fashion from bulk materials. The alternative is the bottom-up approach in which the nano-scale contact between a single molecule (i.e., a spin) and probes is controlled.

Figure 2 shows the schematic of the solid-state nuclear-spin array on a substrate fabricated in the bottom-up approach. The each nuclear spin is connected to the source and drain electrodes for the selective detection of the nuclear spin states from the current measurements. The operations on nuclear spins are carried out using the rotating magnetic field, like in the liquid state NMR. The selectivity in the solid-state nuclear-spin array is achieved by the selective modulation of the resonance frequencies using the probes. The details for the detection and operation using the probes, which is the main topic in this chapter, will be described in the later section. Before the detail explanation of the solid-state nuclear-spin system, the brief introduction of a single molecular junction is given in the next section.

4. Single molecular junctions

4.1 Measurements of the conductance in single molecular junctions

The single molecular junction is composed of electrodes and a single molecule sandwiched in between the electrodes. The single molecular junction designed for an atomic-scale diode was originally proposed by Aviram and Ratner in 1974 (Aviram & Ratner, 1974). After 23 years from the pioneering theoretical proposal, an experimental work on a single molecular junction was firstly reported by Reed and co-workers in 1997 (Reed et al., 1997), in which a single benzen-1,4-dithiolate molecule was sandwiched between gold electrodes. They used mechanically controllible break junction (MCBJ) technique to fabricate the single molecular junction, and measured the electronic current through the junction. In the MCBJ technique (Ruitenbeek et al., 2005), a notch cut on the bulk electrode will be the breaking position by the push-and-pull breaking motion of the electrodes, and thereby a single molecular junction will be obtained at this breaking position (see Figure 6(a)). However, the length of the notch on the electrode may spread over the macro scale, and thus it is sometimes quite difficult to confirm that the number of the molecule sandwiched between the electrodes is exactly one. The break junction technique thus has been improved to be more precise method, and one of the experimental technique frequently used now is the break junction using the scanning tunneling microscope (STM) (Cui et al., 2001; Xu & Tao, 2003). We call it STM-BJ method. Since the length scale of the apex of the STM probe carefully prepared is in the nano-scale, the STM-BJ technique is more suitable for the fabrication and current measurements of the single molecular junctions (see Figure 6(b)). Like in MCBJ, the STM-tip is pushed or pulled to fabricate the single molecular junction.

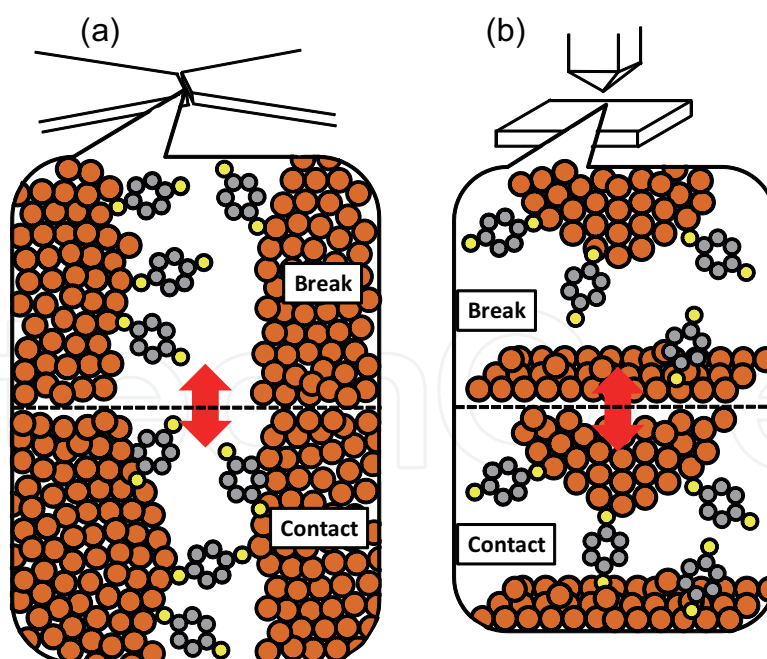


Fig. 6. Schematics of single molecular junctions fabricated during the push-and-pull motion of electrodes in (a) MCBJ and (b) STM-BJ techniques. The blown atoms represent electrodes, and a tiny structure composed of the gray and yellow atoms represents a single molecule.

Even for the STM-BJ technique, we still have the question that the number of the molecule sandwiched between the STM probe and substrate is exactly one or not. The standard strategy

to distinguish the number of sandwiched molecules is the tracing of the measured current during the pulling motion of the STM-tip. Figure 7(a) shows the typical trace of the measured conductance, in which we can confirm several plateaus followed by a drop. If there is no bridge (i.e., a molecule) between the STM-tip and substrate, we can expect the current of zero. Thus the last plateau indicated with an arrow in Fig. 7(a) is the signature of the single molecular chain or atomic chain sandwiched between the electrodes. Since the conductance values of the single molecular junctions are typically less than $0.1 G_0$, and those of the atomic chain of metal larger than $1.0 G_0$ in general, we can speculate the presence of the single molecule between electrodes from the value of the conductance; G_0 is the quantum unit of conductance, $2e^2/h$.

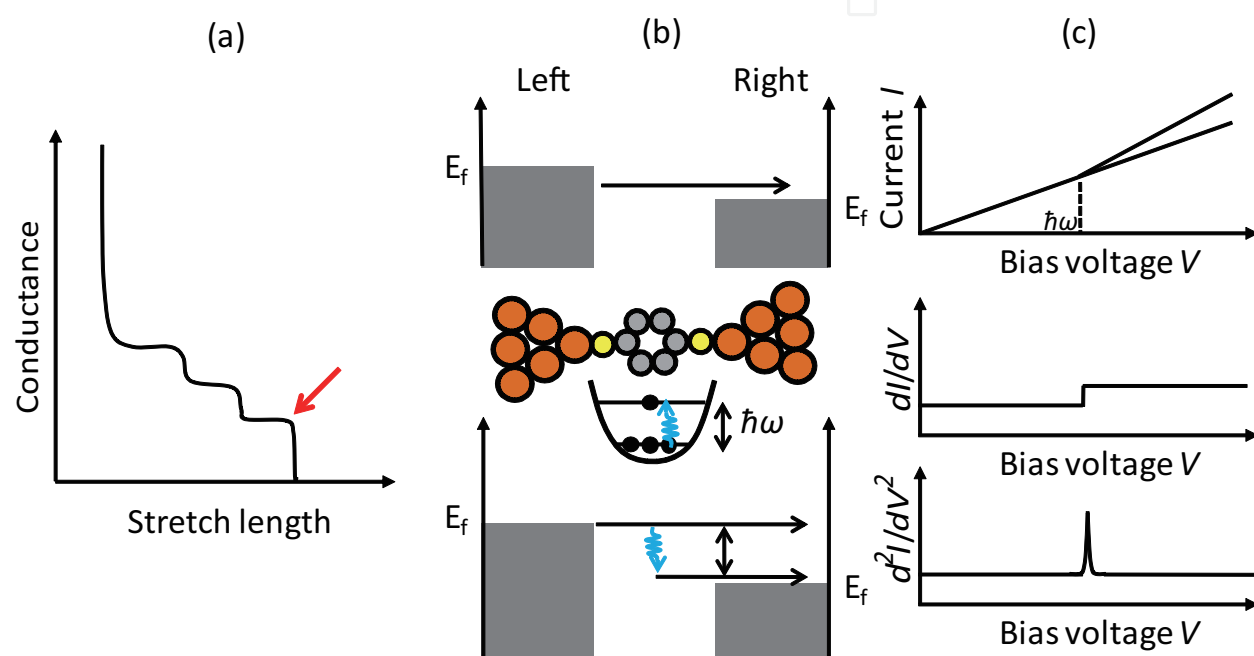


Fig. 7. Schematics of (a) conductance traces, (b) an inelastic process accompanied by the excitation of molecular vibration, and (c) IETS spectra.

To determine the presence of the single molecule between electrodes more precisely, we can use inelastic electron tunneling spectroscopy (IETS). In the IETS measurements, the signature of the single molecule appears as a sharp peak in the d^2I/dV^2 spectrum at the energy of molecular vibration (Ruitenbeek, 2010; Wang et al., 2005). The appearance of the peak is comprehensible as follows: when the applied bias voltage becomes larger than the vibration energy of the single molecule, the inelastic tunneling process accompanied by the excitation of molecular vibration (Fig. 7(b)) is added to the total tunneling current, leading to the abrupt enhancement of the tunneling current at the voltage. This enhancement results in the step in dI/dV and the sharp peak in d^2I/dV^2 (Fig. 7(c)).

Using these experimental techniques, STM-BJ and IETS, the measurements of single molecular junctions have been reported for many kinds of molecules (e.g., hydrogen molecule, saturated hydrocarbon chains, π conjugated organic molecules, DNA molecules, and so on.) (Metzger, 2005; Porath et al., 2005; Ruitenbeek et al., 2005; Wang et al., 2005). In addition to the sophisticated experimental method, the theoretical computations for the conductance of the

single molecular junctions have been developed and applied in order to understand the experimental results precisely. As for the theoretical methods for conductance calculation, there are many types of theoretical frameworks; scattering wave function method (Choi & Ihm, 1999; Gohda et al., 2000; Smogunov et al., 2004), Lippmann-Schwinger equation (Emberly & Kirczenow, 1999; Lang, 1995), the recursion-transfer-matrix method (Hirose & Tsukada, 1994; 1995), and non-equilibrium Green’s function (NEGF) method (Brandbyge et al., 2002; Taylor et al., 2001) are the frequently adopted methods. In the next section, the NEGF and wave-packet scattering methods for conductance calculations in the coherent regime are described.

4.2 Conductance calculations in single molecular junctions

4.2.1 Wave-packet scattering approach

In this section, we consider how we can calculate the electronic conductance in molecular nano-scale junctions. We focus our attention on a one-dimensional system in which the Hamiltonian is written in the tight-binding framework in order to represent the scattering events caused by the sandwiched molecule.

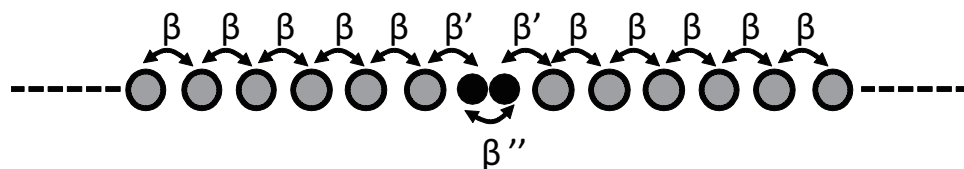


Fig. 8. One-dimensional diatomic molecular junction. The black dots are the single diatomic molecule sandwiched between the one-dimensional electrodes.

Figure 8 shows the one-dimensional molecular junction in which the diatomic molecule is sandwiched in between the one-dimensional electrodes. In the tight-binding model with the hopping integrals β, β', β'' and on-site energy α, α' , the Hamiltonian matrix can be written as

$$\mathbf{H} = \begin{pmatrix} \mathbf{H}_e & \mathbf{t}^\dagger & \mathbf{0} \\ \mathbf{t} & \mathbf{H}_c & \mathbf{t}^\dagger \\ \mathbf{0} & \mathbf{t} & \mathbf{H}_{e'} \end{pmatrix} \tag{3}$$

where

$$\mathbf{H}_e = \begin{matrix} \dots & i-1 & i & i+1 & i+2 & \dots \\ \vdots & \ddots & \ddots & \ddots & & \\ i-1 & \ddots & \alpha & -\beta & & \\ i & \ddots & -\beta & \alpha & -\beta & \\ i+1 & & -\beta & \alpha & -\beta & \ddots \\ i+2 & & & -\beta & \alpha & \ddots \\ \vdots & & & & \ddots & \ddots & \ddots \end{matrix}, \tag{4}$$

$$\mathbf{H}_c = \begin{pmatrix} \dots & m-2 & m-1 & m & m+1 & m+2 & m+3 & \dots \\ \vdots & \ddots & \ddots & & & & & \\ m-2 & \ddots & \alpha & -\beta & & & & \\ m-1 & & -\beta & \alpha & -\beta' & & & \\ m & & & -\beta' & \alpha' & -\beta'' & & \\ m+1 & & & & -\beta'' & \alpha' & -\beta' & \\ m+2 & & & & & -\beta' & \alpha & -\beta \\ m+3 & & & & & & -\beta & \alpha & \ddots \\ \vdots & & & & & & & & \ddots & \ddots \end{pmatrix}, \quad (5)$$

and

$$\mathbf{t} = \begin{pmatrix} \dots & 0 & -\beta \\ & & 0 \\ & & \vdots \end{pmatrix}. \quad (6)$$

In these matrix elements, i is the site number in the one-dimensional electrode, and m and $m+1$ are the sites of the sandwiched molecule. The on-site energy α and hopping integral in electrodes β are respectively set to be 0 and 1. Let us firstly explain the dynamics of a wave-packet scattered by the sandwiched molecule using the wave-packet propagation. Since we can straightforwardly understand the scattering process in the wave-packet dynamics, the comparison between the results from the wave-packet and Green's function is useful to understand what is expressed in Green's function method.

Using the Hamiltonian matrix, we can propagate the wave-packets in the Crank-Nicholson scheme (Press et al., 1992), in which the norm of the wave-packet is completely conserved.

$$\psi(x_i, t + \Delta t) = \frac{1 + \frac{1}{i\hbar} \frac{\Delta t}{2} H}{1 - \frac{1}{i\hbar} \frac{\Delta t}{2} H} \psi(x_i, t). \quad (7)$$

This expression is straightforwardly derived from the time-dependent Schrödinger equation. The number of the sites in the whole system is 2,000 in total. As for the initial wave-packet, we constructed the Gaussian packets from the eigenvectors of the one-dimensional electrode.

Figure 9 shows a typical wave-packet dynamics in the one-dimensional molecular junction, in which the energy of the wave-packet is set to be the Fermi level E_f of the electrode. The velocity of the initial wave-packet is oriented to the right direction. When the packet reaches the sites of the diatomic molecule, m and $m+1$ (the dots in Fig. 9), a portion of the packet is reflected or transmitted by the presence of the hopping integral β' . Counting the amplitudes of transmitted packet in the right electrode, we can calculate transmission probabilities as a function of the energy as

$$T(E) = \frac{\sum_{i \in R} |\psi^E(x_i, t_1)|^2}{\sum_{i \in L} |\psi^E(x_i, t_0)|^2}, \quad (8)$$

where L/R is respectively the left/right electrode and E is the energy of the propagating wave-packet. t_0 is the initial time, and t_1 is an arbitrary time after the transmission and reflection events (e.g., 50 fs in Fig. 9).

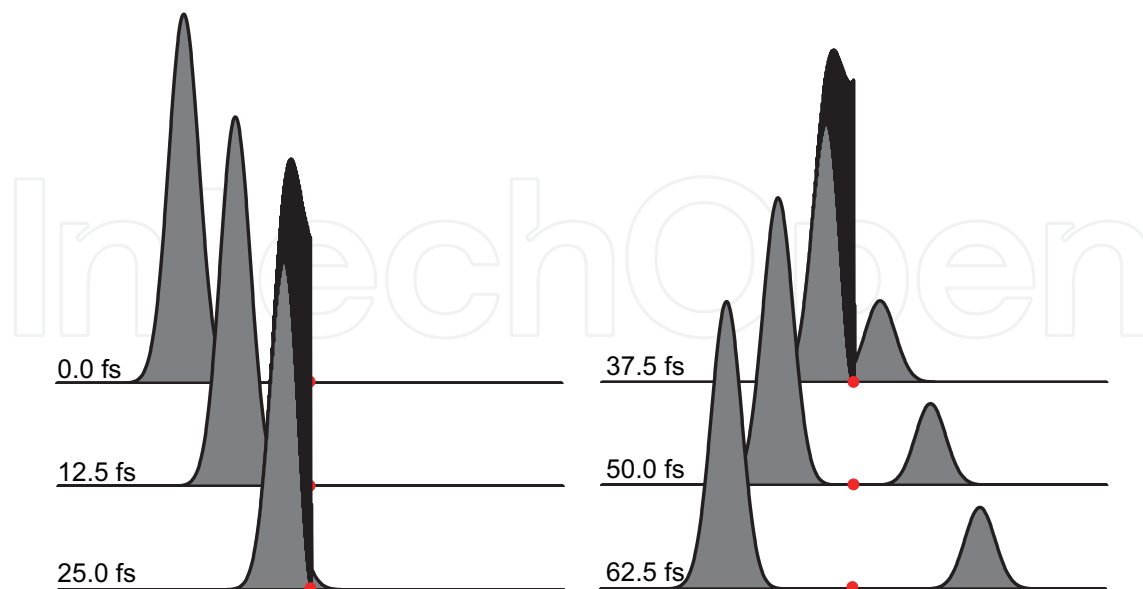


Fig. 9. Simulated wave-packet propagation in the tight binding one-dimensional molecular junction. The tight-binding parameters adopted in the propagation are 0.5β for β' , 1.0β for β'' , and 0 for α' . The red dots indicate the position of the diatomic molecule.

We calculate the electronic conductance using the transmission probability as

$$G = \frac{1}{V} \frac{2e}{h} \int_{E_f - eV/2}^{E_f + eV/2} dE T(E). \quad (9)$$

When the energy dependence on the transmission probability is negligibly small, the Ladauer's formula for conductance is obtained as

$$G = \frac{2e^2}{h} T(E_f). \quad (10)$$

The calculation of transmission probabilities is thus the key in the calculations of the conductance in molecular junctions.

4.2.2 Green's function approach

In this section we also adopted the same molecular junction used in the previous section, and thereby the matrix elements are also the same in Eqs. 3-6. Since the details of the relationship between the wave functions and Green's functions are described in many sophisticated text books (Bruus & Flensberg, 2004; Datta, 1997; 2005; Haug & Jauho, 1998; Stokbro et al., 2005; Ventra, 2008), we focus only on the important equations in Green's function approach for conductance in this section.

In the matrix representation of Green's function approach for electronic conduction, the transmission probability is represented as

$$T(E) = \text{Tr}[i\{\Sigma_L^R(E) - \Sigma_L^A(E)\}G^R(E)i\{\Sigma_R^R(E) - \Sigma_R^A(E)\}G^A(E)], \quad (11)$$

where $\mathbf{G}^{A/R}$ is the advanced/retarded Green's functions describing the scattering processes, and $\Sigma^{A/R}$ is the advanced/retarded self-energies including the interactions between the molecular region and electrodes; the subscript L/R means the left/right electrodes and the advanced functions are the Hermitian conjugate of the corresponding retarded functions. The matrix expressions for these functions are

$$\mathbf{G}^R(E) = [\mathbf{E}\mathbf{1} - \mathbf{H}_{mol} - \Sigma_L^R(E) - \Sigma_R^R(E)]^{-1} \quad (12)$$

and

$$\Sigma^R(E) = \mathbf{t}\mathbf{g}^R(E)\mathbf{t}^\dagger, \quad (13)$$

where \mathbf{g} is the surface Green's function of the electrode, which is obtained with a recursive method. In the simple one-dimensional junction shown in Fig. 8, the matrix \mathbf{H}_{mol} is the 2×2 matrix in the basis of m and $m+1$ and the matrix elements in the 2×2 self energies are

$$(\Sigma_L^R)_{ij}(E) = \beta'^2 g^R(E) \delta_{ij} \delta_{i1} \quad (14)$$

and

$$(\Sigma_R^R)_{ij}(E) = \beta'^2 g^R(E) \delta_{ij} \delta_{i2}, \quad (15)$$

where the surface Green's function of the one-dimensional electrode g can be expressed in the analytical form (Emberly & Kirczenow, 1999) as

$$g^R(E) = \frac{i}{2\beta'} \frac{1 - \exp[i2y_0(E)]}{\sin y_0(E)} \quad (16)$$

and

$$y_0(E) = \arccos(E/2\beta'). \quad (17)$$

Using the Green's functions, we calculated the transmission probabilities of the one-dimensional molecular junction. Figure 10 shows the calculated transmission probabilities, together with those calculated from the wave-packet scattering approach. Both methods show the same transmission probabilities and we thus understand that the scattering event described in wave-packet approach is exactly represented in Green's function approach.

4.2.3 Nonequilibrium Green's function approach in the framework of the first-principles method

Let us briefly describe the conductance calculations in the nonequilibrium Green's function approach within the framework of the first-principles methods, especially for what is modified and what is added compared with the simple tight-binding framework. The major differences are listed as follows:

- (i) We have to solve the scattering problems using non-orthogonal basis sets, which are generally used in the first-principles method.
- (ii) Many non-diagonal elements show non-zero values because of the more spreading basis sets in the first-principles method.
- (iii) The matrix elements depend on the electron densities, and we thus have to determine the electron densities in a self-consistent manner.

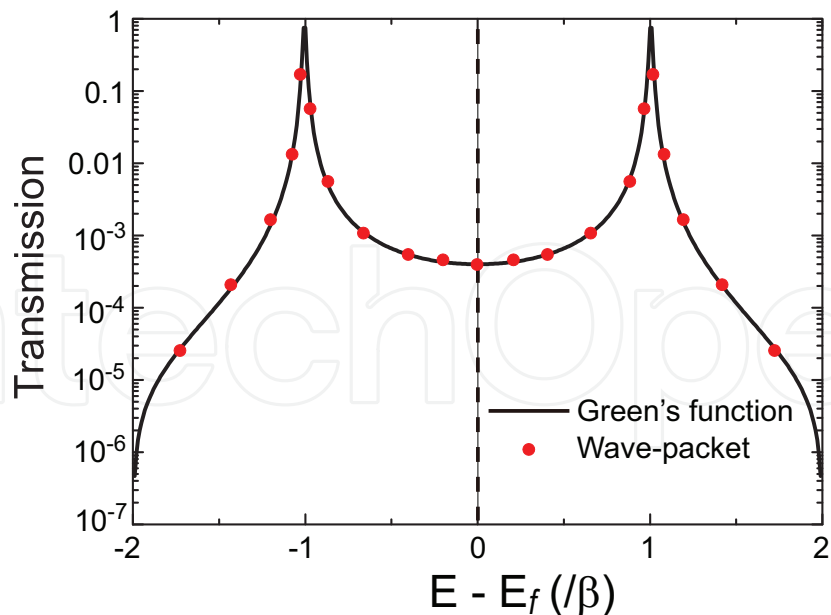


Fig. 10. Calculated transmission probabilities of the one-dimensional molecular junction. The solid line is obtained using Green's function method, and symbols (dots) are wave-packet scattering approach. The tight-binding parameters adopted in these calculations are the same to those in Fig. 9: 0.5β for β' , 1.0β for β'' , and 0 for α' .

(iv) The electrostatic potential has to be determined to hold the boundary conditions.

Since the Green's function in the non-orthogonal basis sets is expressed as $\mathbf{G}(E) = [\mathbf{E}\mathbf{S} - \mathbf{H}_{mol} - \mathbf{\Sigma}_L(E) - \mathbf{\Sigma}_R(E)]^{-1}$ using the overlap matrix \mathbf{S} , the first point is trivial. This is also true for the Green's functions of electrodes. In Point (ii), we have to take care in the matrix division so as not to having non-zero elements in the non-diagonal positions between the left and right electrodes. Thereby the scattering (i.e., molecular) region sandwiched between the two electrodes must be larger than that in the simple tight-binding model where the matrix size of \mathbf{H}_{mol} is 2×2 . In general, the scattering region includes several metallic atoms/layers. The appropriate size of the scattering region is determined by confirming that the calculated result does not depend on the adopted size of the scattering region. As for Point (iii), we have to take care that the electron density is represented by the lesser Green's function $\mathbf{G}^< (= i\mathbf{G}^R[i(\mathbf{\Sigma}_L^R - \mathbf{\Sigma}_L^A)f_L + i(\mathbf{\Sigma}_R^R - \mathbf{\Sigma}_R^A)f_R]\mathbf{G}^A)$, where $f_{L/R}$ is the Fermi distribution function of the left/right electrode, respectively. The density matrix ρ of the scattering region is calculated using the lesser Green's function as

$$\rho = \int dE \frac{-i}{2\pi} \mathbf{G}^<(E). \quad (18)$$

When the two Fermi distribution functions have the same value, the lesser Green's function can be represented with the retarded Green's function as $-i\mathbf{G}^< = \text{Im}[\mathbf{G}^R]$. Since the retarded Green's function has the analytic continuity property, the numerical integral with respect to energy in Eq. 18 can be extensively reduced by means of the contour integral on the complex plane (Taylor et al., 2001). The energy integral in Eq. 18 is thus divided into two parts: (i) the complex contour integral in the energy range out of the bias windows and (ii) the integral on the real axis in the bias window. The submatrix inversion method will be useful for the design

of the contour path when the core/semi-core states are included in the calculations (Tada & Watanabe, 2006). In Point (iv), the Poisson equation with appropriate boundary conditions is solved, and the voltage drop over the sandwiched molecule is reasonably determined.

5. Operation-readout robust switching for the single nuclear spin qubit

5.1 Readout from current measurements

Now that we have introduced the computational tools for the calculations of the conductance of the single molecular junctions, let us consider the application for the quantum computers constituted by the single molecular junctions. Since we consider the nuclear spin qubit for quantum computations in this chapter, the single molecular junction must include a nuclear spin, and we thus regard each qubit in Fig. 2 as a single atom with the nuclear spin of $\frac{1}{2}$.

Figure 11 shows the concept of the readout of a nuclear spin state in tunneling current measurements. The keys in the readout are the hyperfine interactions between the nuclear and tunneling electron spins and the inelastic tunneling current caused by the hyperfine interactions. Assuming that the spin of the incoming electron is polarized as down-spin ($s_z = -\frac{1}{2}; -$) by spin valve α , we expect the following tunneling processes: (i) when the nuclear spin I_z is equal to $\frac{1}{2}$ (up-spin; +), a new conduction channel of the tunneling electron opens through the spin flip of $|s_z I_z\rangle = |- +\rangle \rightarrow |+ -\rangle$ when applied bias voltage is larger than the Zeeman energy $\hbar\omega_0$ of the nuclear spin, resulting in the inelastic current with up-spin (Fig. 11(a)), and (ii) when the nuclear spin I_z is equal to $-\frac{1}{2}$ (down-spin), spin flip does not occur because of the spin conservation, leading to the elastic current with down-spin only (Fig. 11(b)). The inelastic process in the former case is comprehensible in the analogy of IETS described in Section 4. Note that we also assumed that there are no localized electron spins in the single nuclear spin-flip (SNuSF) region, and that nuclei in electrodes (i.e., source/drain electrodes) have no nuclear spins to avoid unexpected spin-flip processes. Thus the detection of tunneling current with up-spin in the drain electrode is the proof of the nuclear spin I_z of $\frac{1}{2}$. The detection of the tunneling electron with up-spin can be achieved by using another spin valve β in the drain electrode. Since the event we should detect is the single spin-flip process, the measured current accompanied by the spin-flip must be originated from the single electron tunneling at most. This is a clear difference from IETS for the detection of the molecular vibrations. Thus the spin valves connected to the single molecular junction is essentially important in the determination of nuclear spin states from tunneling current measurements.

5.2 Initialization through dynamic nuclear polarization

In order to confirm the plausibility of the electron-nuclear spin-flip process, we consider a situation where a bias voltage is applied to all the pairs of the source and drain electrodes in the single nuclear spin array (Fig. 2). Since the appropriate spin valves α and β are connected to the spin array and the spins of the incoming electrons passing through valve α are perfectly polarized, the spin-flip process shown in Fig. 11(a) occurs only for the nuclei with up-spin by waiting an enough time for the spin-flip process. Once the spin-flip occurs, the spin-flipped nucleus has the down-spin, and the spin-flip process for the nucleus is not expected to occur any more. That is, all the nuclear spins will be polarized to the down-spin by the bias

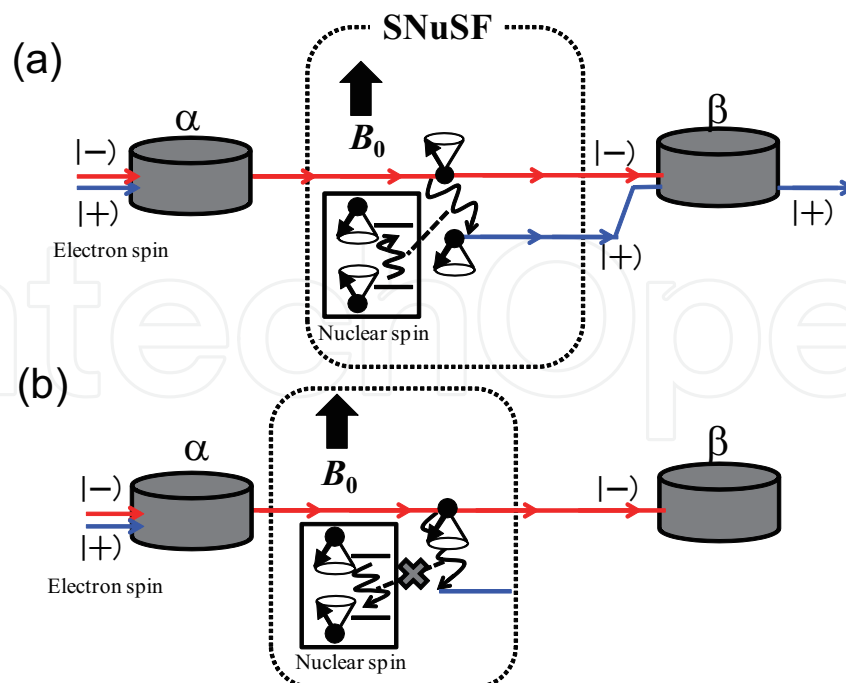


Fig. 11. Basis concept in the readout of the nuclear spin states from current measurements. The red and blue arrows represent the down and up spins of conduction electrons, respectively. The inelastic processes are allowed for (a) the nucleus with up-spin and forbidden for (b) the nucleus with down-spin.

application as shown in Fig. 12. This is the dynamic nuclear polarization by applying the bias voltage in the one-dimensional nuclear spin array.

The dynamic nuclear polarizations by the spin current or in spin-selective systems have already been confirmed in quantum dots, silicon substrates including phosphorus, and NV centers in diamond; the reported polarization rate is 38 – 52 % in quantum dots (Baugh et al., 2007; Petta et al., 2008), 68 % in phosphorus in silicon (McCamey et al., 2009), and 98 % in NV centers in diamond (Jacques et al., 2009). These experimental observations thus guarantee the plausibility of the electron-nuclear spin-flip process discussed in this chapter. The dynamic nuclear polarization in the one-dimensional nuclear spin array is thus quite useful for the initialization process in a large number of qubits.

5.3 Operations in a selective manner

In the previous sections for the readout and initialization, we did not mention what the enough time for the single nuclear spin-flip is. In fact, this will be described using the first-principles NEGF calculations in the later section, but the point we should stress here is that we can create a special situation where the nuclear spin does not experience the spin-flip (i.e., the nuclear-spin conserved situation) even when we apply a bias voltage to the target nucleus. Note that the probability of the nuclear spin-flip is the issue of the spin-flip time: If the spin-flip time is long enough, the nucleus is lying on the situation of the spin conserved, and if it is short the nuclear spin states will be influenced by tunneling current (i.e., the readout situation). We will explain in the later section that these two situations can be exchanged in a simple way. Anyway, this section is devoted to explain how the operations for qubits are

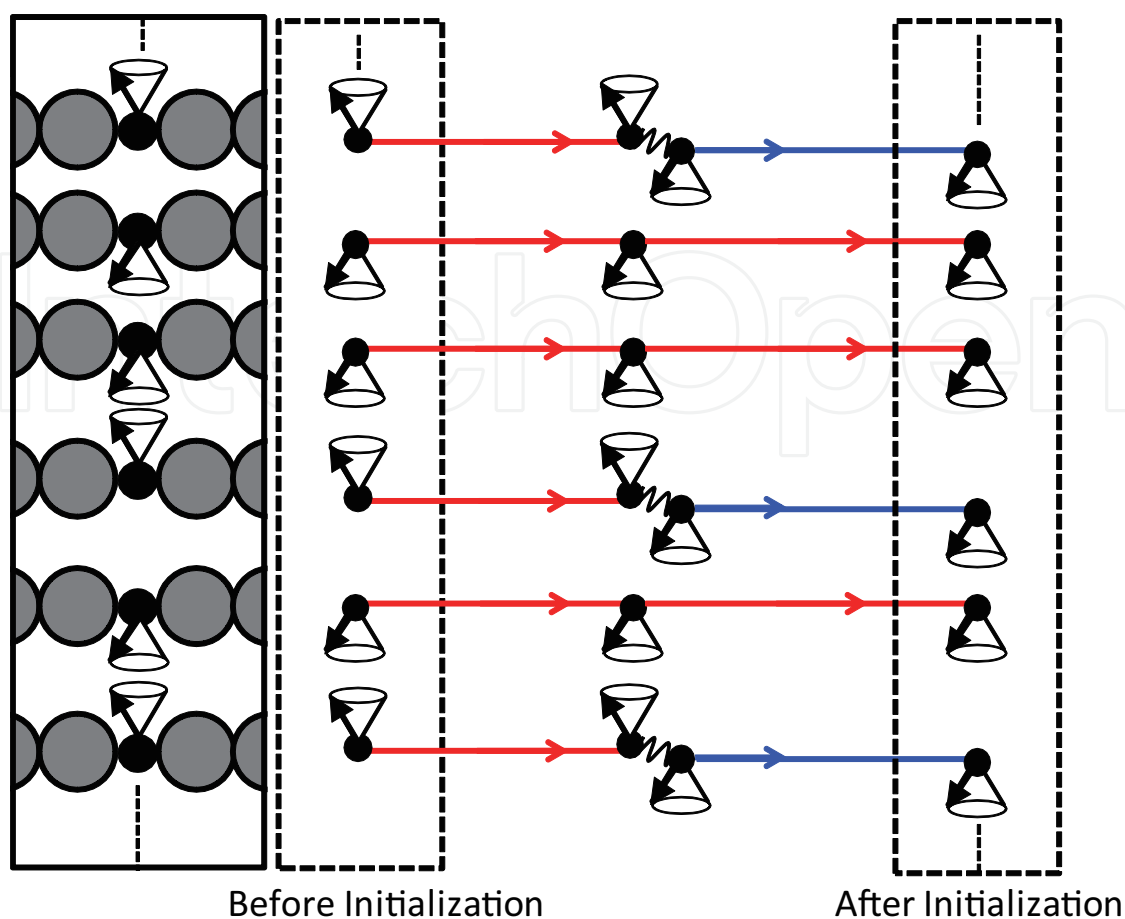


Fig. 12. Dynamic nuclear polarization in the one-dimensional spin array. The nuclear spins are all polarized to the down-spin after the bias applications.

carried out in a selective manner. The nuclear-spin conserved situation is essential for the selective operations.

Figure 13 shows the schematic of the selective operations. The key in the selective operations is that the nuclear-spin conserved situation is realized by applying the *gate* bias voltages even when we apply the source-drain bias voltage to the target nucleus. Although the nucleus does not experience the spin-flip, the nucleus feels an important influence from the bias application. The influence is the redistribution of electron densities around the nucleus, and the redistribution will lead to a modulation of the frequencies for the nuclear magnetic resonance (NMR) with respect only to the target nucleus, that is, the bias induced chemical shift of NMR. In general, the chemical shift of NMR is determined by the chemical environment, but in the nuclear spin array device we can selectively tune the chemical shift of the target nucleus (qubit) by applying the bias voltage to the electrodes connected to the qubit (Fig. 13). Using a rotating magnetic field of the modulated frequency for the target qubit, we can control the spin direction of the target qubit only (i.e., the unitary operation). The c-NOT operation for a pair of the neighboring qubits will be possible by applying the bias voltage to the pair of electrodes connected to the target qubits. The plausibilities of the selective operations explained here are discussed using the first-principles NEGF calculations in the later section.

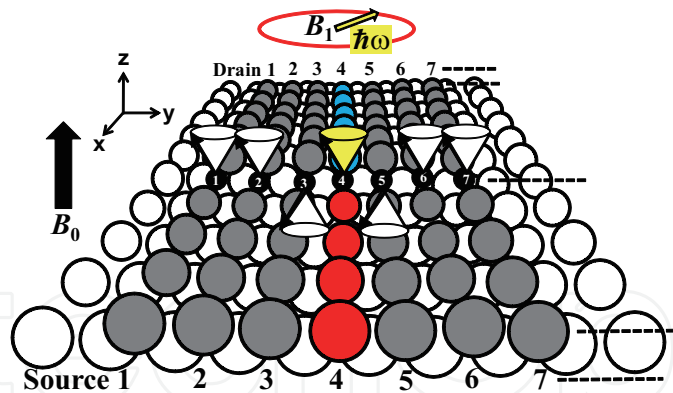


Fig. 13. Schematic of the selective operation. The bias voltage is applied to the electrodes connected to the 4-th qubit to modulate the resonance frequency of the qubit.

5.4 Nonequilibrium Green's function calculations for the robust switching between operation and readout

5.4.1 Computational method

The main issue in the selective readout and operations is the probability of the single nuclear spin-flip process by hyperfine interactions with a spin polarized tunneling electron as described in the previous section. In hyperfine interactions, the relaxation of nuclear spin \mathbf{I} is mainly caused by the scalar contact and dipolar interactions with electron spin \mathbf{S} , which are represented as

$$\mathcal{H}^{sc} = -\frac{2\mu_0}{3}\gamma_e\gamma_n\hbar^2\delta(0)(\mathbf{S} \cdot \mathbf{I}) \quad (19)$$

and

$$\mathcal{H}^{di} = -\frac{\mu_0}{4\pi}\gamma_e\gamma_n\hbar^2\left\{\frac{\mathbf{S} \cdot \mathbf{I}}{r^3} - \frac{3(\mathbf{S} \cdot \mathbf{r})(\mathbf{I} \cdot \mathbf{r})}{r^5}\right\}, \quad (20)$$

respectively. γ_e and γ_n are respectively the gyromagnetic ratios of free electron and nucleus, and r is the distance from the target qubit. Note that the target qubit is positioned at the origin in the coordinate. When a bias voltage V is applied to the SNUF system, the probability w of the nuclear spin-flip by tunneling electron can be written as,

$$w_{(-+)\rightarrow(+)} = \int_{-\infty}^{\infty} dE \frac{2\pi}{\hbar} |\langle \Psi^{+-}(E) | \mathcal{H}^{sc} + \mathcal{H}^{di} | \Psi^{-+}(E') \rangle|^2 \delta(E - E') \times f_L(E) \{1 - f_R(E)\}, \quad (21)$$

where Ψ^{-+} is a product state of a scattering wave function with down-spin ψ^- and spin function of nucleus with up-spin (Tada, 2008). The fermi distribution functions of the left (right) electrodes $f_{L(R)}$ in Eq. (21) guarantee that the spin-flip is caused by tunneling electron in the bias window V . The scattering wave function can be expanded with atomic orbitals ϕ_μ as $\psi^\pm(E, r) = \sum_\mu C_\mu^\pm(E)\phi_\mu(r)$, and thus the matrix elements for the scalar contact and dipolar interactions in Eq. (21) are proportional to

$$\sum_{\mu\nu} C_\mu^{\pm*}(E) C_\nu^\mp(E) \phi_\mu^*(0) \phi_\nu(0) (\mathbf{S} \cdot \mathbf{I}), \quad (22)$$

and

$$\sum_{\mu\nu} C_{\mu}^{\pm*}(E) C_{\nu}^{\mp}(E) \left\langle \phi_{\mu}(r) \left| \frac{\mathbf{S} \cdot \mathbf{I}}{r^3} - \frac{3(\mathbf{S} \cdot \mathbf{r})(\mathbf{I} \cdot \mathbf{r})}{r^5} \right| \phi_{\nu}(r) \right\rangle, \quad (23)$$

respectively. The indices μ and ν in Eq. (22) run over atomic orbitals having non-zero values at the qubit position. (e.g., 1s, 2s orbitals). In these equations, we have to take care which terms in $(\mathbf{S} \cdot \mathbf{I})$ and $\{\mathbf{S} \cdot \mathbf{I}/r^3 - 3(\mathbf{S} \cdot \mathbf{r})(\mathbf{I} \cdot \mathbf{r})/r^5\}$ contribute to the nuclear spin-flip processes, depending on the direction of the static magnetic field B_0 .

The term $\mathbf{S} \cdot \mathbf{I}$ is equal to $S_x I_x + S_y I_y + S_z I_z$. When the static magnetic field B_0 is directed to the the z-axis, the nuclear spin-flip is caused by $S_x I_x + S_y I_y$ because the term $S_x I_x + S_y I_y$ is equal to $(S_- I_+ + S_+ I_-)/2$ using the step-up and -down operators, $S_+ = S_x + iS_y$ and $S_- = S_x - iS_y$. That is, the half of $\sum_{\mu\nu} C_{\mu}^{\pm*}(E) C_{\nu}^{\mp}(E) \phi_{\mu}^*(0) \phi_{\nu}(0)$ contributes to the spin-flip process of $| - + \rangle \rightarrow | + - \rangle$ in the scalar contact term. On the other hand, the dipolar term has a more complicated form as

$$\begin{aligned} \left\langle \phi_{\mu}(r) \left| \frac{\mathbf{S} \cdot \mathbf{I}}{r^3} - \frac{3(\mathbf{S} \cdot \mathbf{r})(\mathbf{I} \cdot \mathbf{r})}{r^5} \right| \phi_{\nu}(r) \right\rangle &= \mathbf{S} \cdot \mathbf{A}_{dip} \cdot \mathbf{I} \\ &= [S_x \ S_y \ S_z] \\ &\quad \cdot \begin{bmatrix} \langle \frac{r^2-3x^2}{r^5} \rangle_{\mu\nu} & -\langle \frac{3xy}{r^5} \rangle_{\mu\nu} & -\langle \frac{3xz}{r^5} \rangle_{\mu\nu} \\ -\langle \frac{3xy}{r^5} \rangle_{\mu\nu} & \langle \frac{r^2-3y^2}{r^5} \rangle_{\mu\nu} & -\langle \frac{3yz}{r^5} \rangle_{\mu\nu} \\ -\langle \frac{3xz}{r^5} \rangle_{\mu\nu} & -\langle \frac{3yz}{r^5} \rangle_{\mu\nu} & \langle \frac{r^2-3z^2}{r^5} \rangle_{\mu\nu} \end{bmatrix} \cdot \begin{bmatrix} I_x \\ I_y \\ I_z \end{bmatrix}, \quad (24) \end{aligned}$$

where the notation $\langle \ \rangle_{\mu\nu}$ means the integral including the atomic orbitals ϕ_{μ} and ϕ_{ν} . For example, $\langle \frac{r^2-3x^2}{r^5} \rangle_{\mu\nu}$ corresponds to $\langle \phi_{\mu}(r) | \frac{r^2-3x^2}{r^5} | \phi_{\nu}(r) \rangle$. When the static magnetic field B_0 is directed to the the z-axis, the terms we have to calculate are those related to $S_x I_x$ and $S_y I_y$ as describe in the contact term, and the tensor \mathbf{A}_{dip} can be written as

$$\mathbf{A}_{dip}^{B_0:z} = \begin{bmatrix} \langle \frac{r^2-3x^2}{r^5} \rangle_{\mu\nu} & 0 & 0 \\ 0 & \langle \frac{r^2-3y^2}{r^5} \rangle_{\mu\nu} & 0 \\ 0 & 0 & 0 \end{bmatrix}. \quad (25)$$

In the expression, we also use the fact that the term $S_x I_y + S_y I_x$ does not include both of the spin-flip components $S_- I_+$ and $S_+ I_-$.

Using the integrals in Eq. (24) and assuming $C^- = C^+$ in Eqs. (22) and (23), which is a reasonable assumption in a spin polarized current by a small bias application, the nuclear spin-flip probability in Eq. (21) is calculated with the lesser Green's function using the relation: $C_{\mu}^{\pm*}(E) C_{\nu}^{\pm}(E) = \frac{-i}{2\pi} [\mathbf{G}^{<,\pm}(E)]_{\mu\nu}$. In the SCF calculations for applied bias cases, a NEGF code (Tada & Watanabe, 2006; Tada, 2008) incorporated in GAUSSIAN03 (Frisch et al., 2003) was employed.

5.4.2 Computational model

The SNUF system considered in the present work is a simple junction composed of a hydrogen molecule sandwiched between ^{106}Pd one-dimensional metallic electrodes ($^{106}\text{Pd}(1\text{D})\text{-}^1\text{H}_2\text{-}^{106}\text{Pd}(1\text{D})$). Table 1 shows the gyromagnetic ratios of typical nuclei. Since the

probability of the nuclear spin-flip depends also on γ_n (see Eqs. (19) and (20)), we adopted the hydrogen molecular junction showing the highest gyromagnetic ratio. The electrodes composed of ^{106}Pd was selected because ^{106}Pd has no nuclear spin: this is one of the conditions required for SNUF describe in Section 5.1.

nucleus	$\gamma_n (\text{sT})^{-1}$
^1H	2.673×10^8
^7Li	1.040×10^8
^{13}C	0.673×10^8
^{19}F	2.517×10^8
^{31}P	1.083×10^8

Table 1. The gyromagnetic ratios of typical nuclei

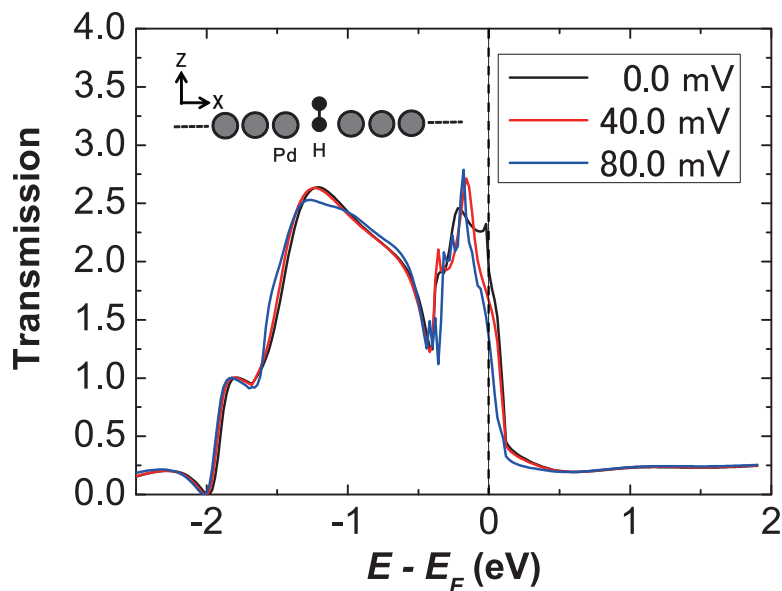


Fig. 14. Calculated transmission functions of the $^{106}\text{Pd}(1\text{D})\text{-}^1\text{H}_2\text{-}^{106}\text{Pd}(1\text{D})$ junction.

We adopted a contact structure in which a hydrogen atom is directly sandwiched between the Pd electrodes as shown in the inset of Fig. 14. Although the adsorption structure is somewhat artificial, we adopted this structure as the first step in the investigation of the nuclear spin-flip probability. The more plausible structures for the hydrogen contact will be investigated in the near future.

5.4.3 Computational results for the robust switching

Figure 14 shows the calculated down-spin transmission function of the Pd(1D)-H₂-Pd(1D) junction in the local density approximation (SVWN functional (Hohenberg & Kohn, 1964; Vosko et al., 1980) in GAUSSIAN 03) of the density functional theory with LANL2MB (Pd) (Hay & Wadt, 1985) and cc-pvdz (H) (Dunning, 1989) basis sets. A sharp peak of transmission function appears below 0.2 eV from the Fermi level E_F in 40 and 80 mV applied bias cases. The peak is also confirmed in three-dimensional Pd electrode systems (Khoo et al., 2008), and thus the shape of the transmission function around the Fermi level is the characteristic property of Pd systems. This is quite important property for the robust switching between the readout (Section 5.1) and operation (Section 5.3) through the control of the hyperfine interaction.

It is well-known that we can modulate the Fermi level of the system by applying the gate bias voltage to the system. When the Fermi level is shifted to the peak level (i.e., $\Delta E_F = -0.2$ eV), the current density of down-spin on the Pd atoms connected to the target hydrogen is significantly enhanced. Since the atomic orbitals of the Pd atoms have non-trivial amplitudes around the target hydrogen, the large electron density in the down-spin current will lead to the enhancement of hyperfine interactions between the nuclear spin and the tunneling current, leading to a fast nuclear spin-flip. The transmission function with up-spin has the same spectra with down-spin, and a conduction channel of up-spin within the bias window opens immediately accompanied by the single nuclear spin-flip process. This is the qubit condition convenient for the selective readout. We use the term *ON-resonance* to express the condition of the Fermi level shifted to the peak position. On the other hand, when the Fermi level is shifted out from the peak level to another level (e.g., $\Delta E_F = 0.1$ eV), we will have a weak hyperfine interaction, leading to an extremely decreased probability of the nuclear spin-flip. This is the qubit condition convenient for the selective operations, because we can rotate the nuclear spins selectively using a rotating magnetic field in this situation as described in Section 5.3. We use the term *OFF-resonance* to express the condition of the Fermi level shifted out from the peak position. Therefore the switching of the hyperfine interactions by shifting the Fermi level will be a robust switching between the readout and operations for qubits in nano-contact systems.

Figure 15 shows the computed spin-flip times (Fig. 15(a)) and significant matrix elements for the scalar contact (Fig. 15(b)) and dipolar interactions (Fig. 15(c)) as a function of the Fermi level shift in 40 mV applied bias case. The spin-flip times clearly depend on the position of the Fermi level: (a) at ON-resonance ($-0.5 < \Delta E_F < -0.1$ eV), the nuclear spin-flip event occurs within 100 - 1000 s because of the enhanced hyperfine interactions, and (b) at OFF-resonance ($0.1 < \Delta E_F < 0.5$ eV), the nuclear spin-flip time is $10^5 - 10^7$ s. The computed spin-flip times indicate that a single nuclear spin-flip in the present molecular junction might be a measurable event at the ON-resonance condition, and that the nuclear spin state is preserved for a long time at the OFF-resonance even when a bias voltage is applied to the single nucleus. The operation-readout robust switching (we call it *hyperfine switching* in the previous study (Tada, 2008)) is strongly related to the electron tunneling through the *d*-orbitals of Pd, as shown in Fig. 15(b,c). The matrix element for the dipolar interaction of *4d* orbital shows the drastic variation around $\Delta E_F = 0.0$ eV, whereas the element for the contact interaction in *2s* orbital of the sandwiched hydrogen shows a moderate variation around $\Delta E_F = 0.0$ eV.

5.4.4 Computational results for the bias induced NMR chemical shifts

The extremely slow relaxation at OFF-resonance is quite useful for the selective operations on NMR qubits as described in Section 5.3. To confirm the modulation of resonance frequency by bias voltage applications at OFF-resonance, the magnetic shielding constant of the target hydrogen in Pd(1D)-H₂-Pd(1D) is calculated using the gauge invariant atomic orbital (GIAO) method (Lee et al., 1995) implemented in the GAUSSIAN03 code. The calculations of shielding constants for Pd(1D)-H₂-Pd(1D) with 40 mV bias application were performed as follows: (i) Hamiltonian matrix of the scattering region (Pd₆-H₂-Pd₆) is calculated from the converged lesser Green's function (density matrix), (ii) molecular orbitals (MOs) for the scattering region are calculated through diagonalization of the Hamiltonian matrix, leading to a set of discrete MO levels, (iii) confirm that the Fermi level used in NEGF calculations is positioned between

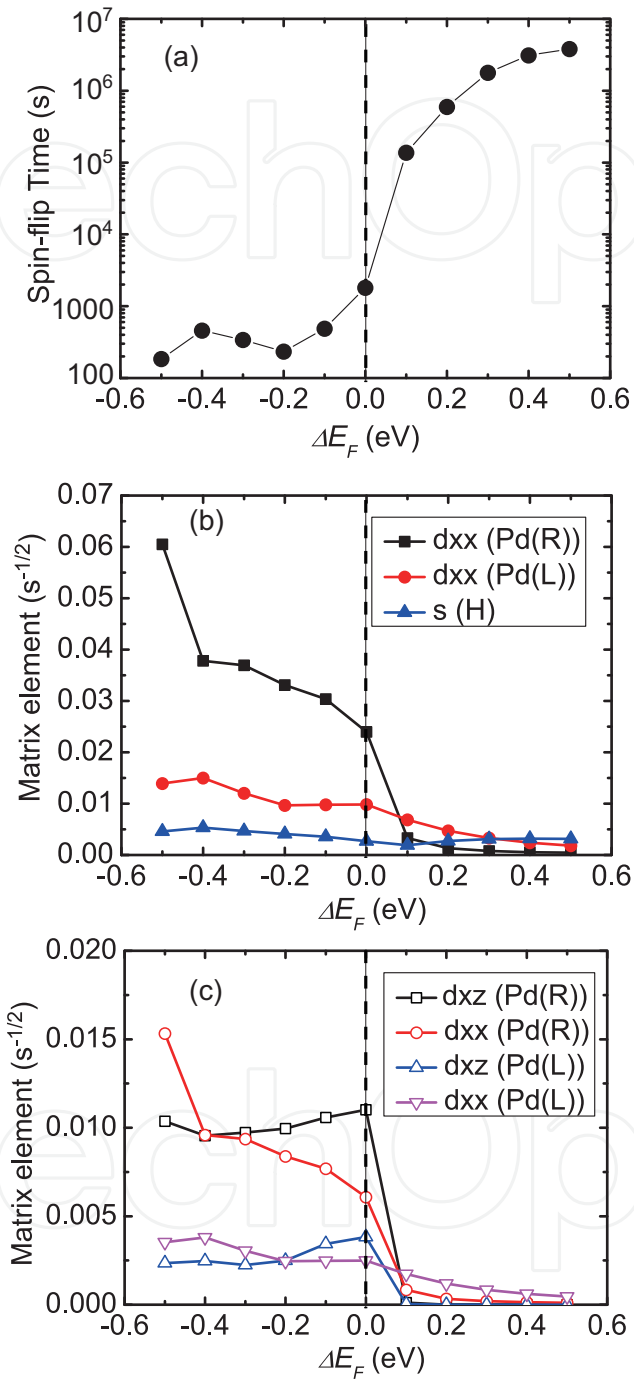


Fig. 15. (a) Computed spin-flip times and (b) significant elements for scalar contact and (c) dipolar interactions as a function of the Fermi level shift ΔE_F .

the highest occupied MO and the lowest unoccupied MO, and (iv) shielding constants are calculated using the discrete MOs in GIAO method. When a magnetic field of 10 T is applied to the SNUF system, the Larmor frequency $\omega_0/2\pi$ (reference frequency) of proton is 425.7 MHz. The calculated shielding constants of the proton for 0.0 and 40.0 mV bias applications are 157.67 and 35.65 ppm, respectively. The frequency shifts from the reference frequency is thus 67.12 and 15.18 kHz for 0.0 and 40.0 mV bias applications, respectively. The difference of the resonance frequency between 0.0 and 40.0 mV bias applications is large enough for selective operations on qubits by making use of radio-frequency pulses (Vandersypen et al., 2001).

5.4.5 The system temperature

In the previous study of *hyperfine switching* for single molecular junctions, the author discussed the cooling down method to prevent unexpected nuclear spin-flips, and the required temperature was estimated to be ~ 10 mK even when the static magnetic field of 10T is applied to the nuclear spin array (Tada, 2008). This requirement is extremely terrible. However, we described the dynamic nuclear polarization technique available for the nuclear spin array in Section 5.2, and we can use this technique in stead of the simple cooling down method. The key property for the system condition using the dynamic nuclear polarization is again the nuclear spin-flip probability depending on the system temperature.

When the system temperature is set to be $T(K)$, the electrons in the energy range from $E_F - k_B T/2$ to $E_F + k_B T/2$ can contribute to the nuclear spin-flip processes (Abragam, 1961), where k_B is the Boltzmann constant. The spin-flip time at $T(K)$ is thus represented as

$$w_{(-+)\rightarrow(+)} = \int_{E_F - k_B T/2}^{E_F + k_B T/2} dE \frac{2\pi}{\hbar} |\langle \Psi^{+-}(E) | \mathcal{H}^{sc} + \mathcal{H}^{di} | \Psi^{-+}(E') \rangle|^2 \delta(E - E'). \quad (26)$$

Here we assumed that the nuclear spins in the array structure are already polarized to the direction of + by the dynamic nuclear polarization. For instance, when the system temperature is equal to the room temperature (300K), the energy window is about 26 meV. Using Eq. 26 and density matrix at the zero bias condition, we obtained the spin-flip time of 1800 s. In addition, using the OFF-resonance conditions induced by the gate bias, the spin-flip time can be extremely long (e.g., $10^5 - 10^7$ s). These results indicate that the nuclear spin states can be preserved in long periods, which are enough for operations and readout.

6. Conclusions

A novel detection mechanism of single nuclear spin-flip by hyperfine interactions between nuclear spin and tunneling electron spin is proposed, and the probability of the nuclear spin-flip is calculated using ab initio non-equilibrium Green's function method. The calculated relaxation times for nano-contact system, Pd(1D)-H₂-Pd(1D), reveal that ON/OFF switching of hyperfine interactions is effectively triggered by resonant tunneling mediated through the d-orbitals of Pd; when the bias voltage of 40 mV is applied to the system, (a) the nuclear spin-flip event occurs within 100 - 1000 s at ON-resonance and (b) the relaxation time of the single nuclear spin-flip is $10^5 - 10^7$ s at OFF-resonance. The effectiveness of bias voltage applications at OFF-resonance for selective operations on qubits is also demonstrated

in the calculations of resonant frequencies of proton using the gauge invariant atomic orbital method.

7. Acknowledgments

This work was partially supported by the Grant-in-Aid for Young Scientists (B), MEXT of Japan.

8. References

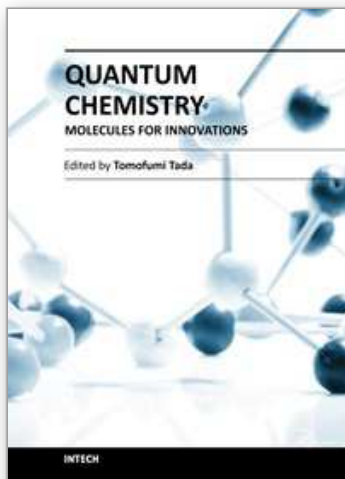
- Abragam, A. (1961). *Principles of Nuclear Magnetism*, Oxford University Press, 019852014X (ISBN), New York.
- Aviram, A. & Ratner, M. A. (1974). Molecular Rectifiers. *Chemical Physics Letters*, 29, 277-283, 00092614(ISSN).
- Baugh, J.; Kitamura, Y.; Ono, K. & Tarucha, S. (2007). Large Nuclear Overhauser Fields Detected in Vertically Coupled Double Quantum Dots. *Physical Review Letters*, 99, 096804(1)-096804(4), 10797114 (ISSN).
- Benenti, G.; Casati, G. & Strini, G. (2004). *Principles of Quantum Computation and Information Volume I: Basic Concepts*, World Scientific, 9812388303 (ISBN), Singapore.
- Bruus, H. & Flensberg, K. (2004). *Many-Body Quantum Theory in Condensed Matter Physics*, Oxford University Press, 0198566336 (ISBN), New York.
- Brandbyge, M.; Mozos, J. L.; Ordejón, P.; Taylor, J. & Stokbro, K. (2002). Density-functional method for nonequilibrium electron transport. *Physical Review B*, 65, 165401(1)-165401(17), 01631829 (ISSN).
- Cappellaro, P.; Jiang, L.; Hodges, J. S. & Lukin, M. D. (2009). Coherence and Control of Quantum Registers Based on Electronic Spin in a Nuclear Spin Bath. *Physical Review Letters*, 102, 21, 210502(1)-210502(4), 10797114 (ISSN).
- Carroll, R. L. & Gorman, C. B. (2002). The Genesis of Molecular Electronics. *Angewandte Chemie International Edition*, 41, 4378-4400, 15213773 (ISSN).
- Childress, L.; Dutt, M. V. G.; Taylor, J. M.; Zibrov, A. S.; Jelezko, F.; Wrachtrup, J.; Hemmer, P. R. & Lukin, M. D. (2006). Coherent dynamics of coupled electron and nuclear spin qubits in diamond. *Science*, 314, 281-285, 00368075 (ISSN).
- Choi, H. J. & Ihm, J. (1999). Ab initio pseudopotential method for the calculation of conductance in quantum wires. *Physical Review B*, 59, 2267-2275, 01631829 (ISSN).
- Cui, X. D.; Primak, A.; Zarate, X.; Tomfohr, J.; Sankey, O. F. Moore, A. L.; Moore, T. A.; Gust, D. Harris, G. & Lindsay, S. M. (2001). Reproducible measurement of single-molecule conductivity. *Science*, 294, 571-574, 00368075 (ISSN).
- Datta, S. (1997). *Electron Transport in Mesoscopic Systems*, Cambridge University Press, 0521599431 (ISBN-10), Cambridge.
- Datta, S. (2005). *Quantum Transport: Atom to Transistor*, Cambridge University Press, 0521631459 (ISBN-10), New York.
- Dunning, T. H. (1989). Gaussian-Basis Sets for Use in Correlated Molecular Calculations. 1. The Atoms Boron through Neon and Hydrogen. *Journal of Chemical Physics*, 90, 1007-1023, 00219606 (ISSN).
- Emberly, E. G. & Kirczenow, G. (1999). Antiresonances in molecular wires. *Journal of Physics: Condensed Matter*, 11, 6911-6926, 09538984 (ISSN).

- Frisch, A.; Frisch, M. J. & Trucks, G. W. (2003). *Gaussian 03 User's Reference*, Gaussian Inc., 0972718702 (ISBN), Carnegie.
- Gohda, Y.; Nakamura, Y.; Watanabe, K. & Watanabe, S. (2000). Self-Consistent Density Functional Calculation of Field Emission Currents from Metals. *Physical Review Letters*, 85, 1750-1753, 10797114 (ISSN).
- Haug, H. & Jauho, A. -P. (1998). *Quantum Kinetics in Transport and Optics of Semi-conductors*, Springer, 3540616020 (ISBN), Heidelberg.
- Hay, P. J. & Wadt, W. R. (1985). Ab initio Effective Core Potentials for Molecular Calculations - Potentials for the Transition-Metal Atoms Sc to Hg. *Journal of Chemical Physics*, 82, 270-283, 00219606 (ISSN).
- Hirose, K. & Tsukada, M. (1994). First-Principles Theory of Atom Extraction by Scanning Tunneling Microscopy. *Physical Review Letters*, 73, 150-153, 10797114 (ISSN).
- Hirose, K. & Tsukada, M. (1995). First-Principles Calculation of the electronic structure for a bielectrode junction system under strong field and current. *Physical Review B*, 51, 5278-5290, 01631829 (ISSN).
- Hohenberg, P. & Kohn, W. (1964). Inhomogeneous Electron Gas. *Physical Review*, 136, B864-B871, 0031899X (ISSN).
- Jacques, V.; Neumann, P.; Beck, J.; Markham, M.; Twitchen, D.; Meijer, J.; Kaiser, F.; Balasubramanian, G.; Jelezko, F. & Wrachtrup, J. (2009). Dynamic Polarization of Single Nuclear Spins by Optical Pumping of Nitrogen-Vacancy Color Centers in Diamond at Room Temperature. *Physical Review Letters*, 102, 5, 057403(1)-057403(4), 10797114 (ISSN).
- Jelezko, F.; Gaebel, T.; Popa, I.; Gruber, A. & Wrachtrup, J. (2004). Observation of Coherent Oscillations in a Single Electron Spin. *Physical Review Letters*, 92, 7, 076401(1)-076401(4), 10797114 (ISSN).
- Jelezko, F.; Gaebel, T.; Popa, I.; Domhan, M.; Gruber, A. & Wrachtrup, J. (2004). Observation of Coherent Oscillation of a Single Nuclear Spin and Realization of a Two-Qubit Conditional Quantum Gate. *Physical Review Letters*, 93, 13, 130501(1)-130501(4), 10797114 (ISSN).
- Joachim, C.; Gimzewski, J. K. & Aviram, A. (2000). Electronics using hybrid-molecular and mono-molecular devices. *Nature*, 408, 541-548, 00280836 (ISSN).
- Kane B. (1998). Silicon-Based Nuclear Spin Quantum Computer. *Nature*, 393, 133-137, 00280836 (ISSN).
- Khoo, K. H.; Neaton, J. B.; Choi, H. J. & Louie, S. G. (2008). Contact dependence of the conductance of H₂ molecular junctions from first principles. *Physical Review B*, 77, 115326(1)-115326(6), 01631829 (ISSN).
- Lang, N. D. (1995). Resistance of Atomic Wires. *Physical Review B*, 52, 5335-5342, 01631829 (ISSN).
- Ladd, T. D.; Jelezko, F.; Laflamme, R.; Nakamura, Y.; Monroe, C. & O'Brien, J. L. (2010). Quantum computers. *Nature*, 464, 45-53, 00280836 (ISSN).
- Lee, A. M.; Handy, N. C. & Colwell, S. M. (1995). The Density-Functional Calculation of Nuclear Shielding Constants using London Atomic Orbitals. *Journal of Chemical Physics*, 103, 10095-10109, 00219606 (ISSN).
- Lo, C. C.; Bokor, J.; Schenkel, T.; He, J.; Tyryshkin, A. M. & Lyon, S. A. (2007). Spin-dependent scattering off neutral antimony donors in field-effect transistors. *Applied Physics Letters*, 91, 242106(1)-242106(3), 00036951 (ISSN).

- McCamey, D. R.; Huebl, H.; Brandt, M. S.; Hutchison, W. D.; McCallum, J. C.; Clark, R. G. & Hamilton, A. R. (2006). Electrically detected magnetic resonance in ion-implanted Si : P nanostructures. *Applied Physics Letters*, 89, 182115(1)-182115(3), 00036951 (ISSN).
- McCamey, D.; van Tol, J.; Morley, G. & Boehme, C. (2009). Fast Nuclear Spin Hyperpolarization of Phosphorus in Silicon. *Physical Review Letters*, 102, 2, 027601(1)-027601(4), 10797114 (ISSN).
- Metzger, R. M. (2005). Six Unimolecular Rectifiers and What Lies Ahead. In: *Introducing Molecular Electronics*, Cuniberti, G.; Fagas, G. & Richter, K. (Ed.), 313-349, Springer, 3540279946 (ISBN-10), Heidelberg.
- Miyano, K. & Furusawa, A. (2008). *An Introduction to Quantum Computation*, Nippon-Hyoron-sha, 9784535784796 (ISBN), Tokyo.
- Morton, J. J. L.; Tyryshkin, A. M.; Brown, R. M.; Shankar, S.; Lovett, B. W.; Ardavan, A.; Schenkel, T.; Haller, E. E.; Ager, J. W. & Lyon, S. A. (2008). Solid-state quantum memory using the ^{31}P nuclear spin. *Nature*, 455, 1085-1088, 00280836 (ISSN).
- Nazin, G. V.; Qiu, X. H. & Ho, W. (2003). Visualization and spectroscopy of a metal-molecule-metal bridge. *Science*, 302, 77-81, 00368075 (ISSN).
- Neumann, P.; Mizuochi, N.; Rempp, F.; Hemmer, P.; Watanabe, H.; Yamasaki, S.; Jacques, V.; Gaebel, T.; Jelezko, F. & Wrachtrup, J. (2008). Multipartite entanglement among single spins in diamond. *Science*, 320, 1326-1329, 00368075 (ISSN).
- Nielsen, M. A. & Chuang, I. L. (2000). *Quantum Computation and Quantum Information*, Cambridge University Press, 0521632358 (ISBN), Cambridge.
- Petta, J. R.; Taylor, J. M.; Johnson, A. C.; Yacoby, A.; Lukin, M. D.; Marcus, C. M.; Hanson, M. P. & Gossard, A. C. (2008). Dynamic Nuclear Polarization with Single Electron Spins. *Physical Review Letters*, 100, 067601(1)-067601(4), 10797114 (ISSN).
- Press, W. H.; Teukolsky, S. A.; Vetterling, W. T. & Flannery, B. P. (1992). *Numerical Recipes in Fortran 77 Second Edition*, Cambridge University Press, 052143064X (ISBN), Cambridge.
- Porath, D.; Lapidot, N. & Gomez-Herrero, J. (2005). Charge Transport in DNA-based Devices. In: *Introducing Molecular Electronics*, Cuniberti, G.; Fagas, G. & Richter, K. (Ed.), 411-444, Springer, 3540279946 (ISBN-10), Heidelberg.
- Reed, M. A.; Zhou, C.; Muller, C. J.; Burgin, T. P. & Tour, J. M. (1997). Conductance of a Molecular Junction. *Science*, 278, 252-254, 00368075 (ISSN).
- Ruitenbeek, J. v.; Scheer, E. & Weber, H. B. (2005). Conducting Individual Molecules using Mechanically Controllable Break Junction. In: *Introducing Molecular Electronics*, Cuniberti, G.; Fagas, G. & Richter, K. (Ed.), 253-274, Springer, 3540279946 (ISBN-10), Heidelberg.
- Ruitenbeek, J. M. v. (2010). Quasi-ballistic electron transport in atomic wires. In: *Oxford Handbook of Nanoscience and Technology: Volume 1: Basic Aspects*, Narlikar, A. V. & Fu, Y. Y. (Ed.), 117-143, Oxford University Press, 0199533040 (ISBN-10), Place of publication.
- Sagawa, H. & Yoshida, N. (2003). *Quantum Information Theory*, Springer Japan, 9784431100560 (ISBN), Tokyo.
- Smeltzer, B.; McIntyre, J. & Childress, L. (2009). Robust control of individual nuclear spins in diamond. *Physical Review A*, 80, 5, 050302(1)-050302(4), 10502947 (ISSN).
- Smogunov, A.; Corso, A. D. & Tosatti, E. (2004). Ballistic conductance of magnetic Co and Ni nanowires with ultrasoft pseudopotentials. *Physical Review B*, 70, 045417(1)-045417(9), 01631829 (ISSN).

- Stegner, A. R.; Boehme, C.; Huebl, H.; Stutzmann, M.; Lips, K. & Brandt, M. S. (2006). Electrical detection of coherent ^{31}P spin quantum states. *Nature Physics*, 2, 835-838, 17452473 (ISSN).
- Stokbro, K.; Taylor, J.; Brandbyge, M. & Guo, H. (2005). Ab-initio Non-Equilibrium Green's Function Formalism for Calculating Electron Transport in Molecular Devices. In: *Introducing Molecular Electronics*, Cuniberti, G.; Fagas, G. & Richter, K. (Ed.), 117-151, Springer, 3540279946 (ISBN-10), Heidelberg.
- Tada, T. & Watanabe, S. (2006). Submatrix Inversion Approach to the ab initio Green's function method for electrical transport. *e-Journal of Surface Science and Nanotechnology*, 4, 484-489, 13480391 (ISSN).
- Tada, T. (2008). Hyperfine switching triggered by resonant tunneling for the detection of a single nuclear spin qubit. *Physics Letters A*, 372, 6690-6693, 03759601 (ISSN).
- Taylor, J.; Guo, H. & Wang, J. (2001). Ab initio modeling of quantum transport properties of molecular electronic devices. *Physical Review B*, 63, 245407(1)-245407(13), 01631829 (ISSN).
- Vandersypen, L. M. K.; Steffen, M.; Breyta, G.; Yannoni, C. S.; Sherwood, M. H. & Chuang, I. L. (2001). Experimental realization of Shor's quantum factoring algorithm using nuclear magnetic resonance. *Nature*, 414, 883-887, 00280836 (ISSN).
- Ventra, M. D. (2008). *Electrical Transport in Nanoscale Systems*, Cambridge University Press, 9780521896344 (ISBN), New York.
- Vosko, S. H.; Wilk, L. & Nusair, M. (1980). Accurate Spin-dependent Electron Liquid Correlation Energies for Local Spin-Density Calculations - A Critical Analysis. *Canadian Journal of Physics*, 58, 1200-1211, 00084204 (ISSN).
- Wang, W.; Lee, T. & Reed, M. A. (2005). Intrinsic Electronic Conduction Mechanisms in Self-Assembled Monolayers. In: *Introducing Molecular Electronics*, Cuniberti, G.; Fagas, G. & Richter, K. (Ed.), 275-300, Springer, 3540279946 (ISBN-10), Heidelberg.
- Xu, B. & Tao, N. J. (2003). Measurement of Single-Molecule Resistance by Repeated Formation of Molecular Junctions. *Science*, 301, 1221-1223, 00368075 (ISSN).

IntechOpen



Quantum Chemistry - Molecules for Innovations

Edited by Dr. Tomofumi Tada

ISBN 978-953-51-0372-1

Hard cover, 200 pages

Publisher InTech

Published online 21, March, 2012

Published in print edition March, 2012

Molecules, small structures composed of atoms, are essential substances for lives. However, we didn't have the clear answer to the following questions until the 1920s: why molecules can exist in stable as rigid networks between atoms, and why molecules can change into different types of molecules. The most important event for solving the puzzles is the discovery of the quantum mechanics. Quantum mechanics is the theory for small particles such as electrons and nuclei, and was applied to hydrogen molecule by Heitler and London at 1927. The pioneering work led to the clear explanation of the chemical bonding between the hydrogen atoms. This is the beginning of the quantum chemistry. Since then, quantum chemistry has been an important theory for the understanding of molecular properties such as stability, reactivity, and applicability for devices. This book is devoted for the theoretical foundations and innovative applications in quantum chemistry.

How to reference

In order to correctly reference this scholarly work, feel free to copy and paste the following:

Tomofumi Tada (2012). Quantum Transport and Quantum Information Processing in Single Molecular Junctions, Quantum Chemistry - Molecules for Innovations, Dr. Tomofumi Tada (Ed.), ISBN: 978-953-51-0372-1, InTech, Available from: <http://www.intechopen.com/books/quantum-chemistry-molecules-for-innovations/quantum-transport-and-quantum-information-processing-in-single-molecular-junctions>

INTECH
open science | open minds

InTech Europe

University Campus STeP Ri
Slavka Krautzeka 83/A
51000 Rijeka, Croatia
Phone: +385 (51) 770 447
Fax: +385 (51) 686 166
www.intechopen.com

InTech China

Unit 405, Office Block, Hotel Equatorial Shanghai
No.65, Yan An Road (West), Shanghai, 200040, China
中国上海市延安西路65号上海国际贵都大饭店办公楼405单元
Phone: +86-21-62489820
Fax: +86-21-62489821

© 2012 The Author(s). Licensee IntechOpen. This is an open access article distributed under the terms of the [Creative Commons Attribution 3.0 License](#), which permits unrestricted use, distribution, and reproduction in any medium, provided the original work is properly cited.

IntechOpen

IntechOpen